

New pulse profile variability associated with a glitch of PSR J0738–4042

S. Q. Zhou,^{1,4,8,9} E. Gügercinoglu,^{2,3*} J. P. Yuan,^{4,10†} M. Y. Ge,⁵ C. Yu,^{1,8,9}
C. M. Zhang,^{2,11,12} J. Zhang,⁶ Z. W. Feng⁷ and C. Q. Ye^{1,9}

¹*School of Physics and Astronomy, Sun Yat-Sen University, Zhuhai, 519082, China*

²*National Astronomical Observatories, Chinese Academy of Sciences, 20A Datun Road, Chaoyang District, Beijing 100101, China*

³*Istanbul University, Faculty of Science, Department of Astronomy and Space Sciences, Beyazıt, 34119, Istanbul, Turkey*

⁴*Xinjiang Astronomical Observatory, Chinese Academy of Sciences, Xinjiang 830011, China*

⁵*Key Laboratory of Particle Astrophysics, Institute of High Energy Physics, Chinese Academy of Sciences, Beijing 100049, China*

⁶*Department of Physics and Electronic Engineering, QiLu Normal University, Jinan 250033, China*

⁷*School of Physics and Astronomy, China West Normal University, Nanchong, 637009, China*

⁸*State Key Laboratory of Lunar and Planetary Sciences, Macau University of Science and Technology, Macau, China*

⁹*CSST Science Centre for the Guangdong-Hong Kong-Macau Greater Bay Area, Zhuhai, 519082, China*

¹⁰*Centre for Astronomical Mega-Science, Chinese Academy of Sciences, Beijing 100012, China*

¹¹*University of Chinese Academy of Sciences, School of Astronomy and Space Science, Beijing 100049, China*

¹²*University of Chinese Academy of Sciences, School of Physical Sciences, Beijing 100049, China*

Accepted XXX. Received YYY; in original form ZZZ

ABSTRACT

The close correlation observed between emission state and spin-down rate change of pulsars has many implications both for the magnetospheric physics and the neutron star interior. The middle-aged pulsar PSR J0738–4042, which had been observed to display variations in the pulse profile associated with its spin-down rate change due to external effects, is a remarkable example. In this study, based on the 12.5-yr combined public timing data from UTMOST and Parkes, we have detected a new emission-rotation correlation in PSR J0738–4042 concurrent with a glitch. A glitch that occurred at MJD 57359(5) (December 3, 2015) with $\Delta\nu/\nu \sim 0.36(4) \times 10^{-9}$ is the first glitch event observed in this pulsar and is probably the underlying cause of the emission-rotation correlation. Unlike the usual post-glitch behaviours, the braking torque on the pulsar has continued to increase over 1380 d, corresponding to a significant decrease in $\ddot{\nu}$. As for changes in the pulse profile after the glitch, the relative amplitude of the leading component weakens drastically, while the middle component becomes stronger. A combined model of crustquake induced platelet movement and vortex creep response is invoked to account for this rare correlation. In this scenario, magnetospheric state-change is naturally linked to the pulsar-intrinsic processes that give rise to a glitch.

Key words: methods: stars: neutron-pulsar: general-pulsars: individual: (PSR J0738–4042).

1 INTRODUCTION

Pulsars are highly-magnetized, rotating neutron stars. Following the discovery of pulsars, the technique known as “pulsar timing” has been naturally used to examine how they rotate. The long-term timing observations have uncovered two types of intrinsic irregularities in the pulsar rotational

evolution: timing noise and glitches. Timing noise in most pulsars is significantly dominated by sustained random wandering in either the phase, spin, or spin-down rate (Boynton et al. 1972; Hobbs et al. 2010; Yuan et al. 2017). Glitches are observed as abrupt increases in the rotation and the spin-down rates of pulsars instantaneous to the accuracy of the data (Palfreyman et al. 2018; Ashton et al. 2019). In general, the post-glitch behaviour is modelled as an initial slow exponential recovery over a few days to several months followed by linear decay of the part of the increase in the spin-down

* E-mail: egugercinoglu@gmail.com

† E-mail: yuanjp@xao.ac.cn

rate on a time-scale of years (Shemar & Lyne 1996; Yuan et al. 2010a; Espinoza et al. 2011; Yu et al. 2013; Liu et al. 2021a; Basu et al. 2022; Gügerciñoğlu et al. 2022b). Pulsar glitches and timing noise can be used to probe into the neutron star internal structure and dynamics (Cheng 1987; Jones 1990; Ho et al. 2015; Sourie & Chamel 2020; Gügerciñoğlu & Alpar 2020; Montoli et al. 2020).

Apart from the above mentioned rotational instabilities cyclic behaviour and switching between two or more states have been reported in increasing number of sources, and in some of them a correlation exists with pulse profile variation. Lyne et al. (2010) demonstrated that for six pulsars the spin-down rate variations are correlated with the pulse shape changes. Periodic modulation in the arrival times of some pulsars is evaluated as being due to precession (Kerr et al. 2016). The first glitch-triggered pulse profile changes were observed in the very young pulsar PSR J1119–6127 (Weltevrede et al. 2011). Recently, Shaw et al. (2022) conducted a search for emission-correlated $\dot{\nu}$ transitions in 17 pulsars previously studied by Lyne et al. (2010) and identified a new correlation in PSR B1642–03. At present, radiative changes accompanied by timing irregularities are extremely rare in pulsars, except for the well-established case of magnetars (Dib & Kaspi 2014; Manchester 2017). This may be, in part due to the comparatively low quality of the available data on many pulsars (low observational cadence, low S/N), resulting in inability to detect the correlated slight variations in their rotational and emission properties.

Table 1 contains the detailed parameters for each observed emission-rotation correlation in thirteen normal pulsars known to us. Their emission mode-changing features – sudden changes to the pulse profile shape or the total flux density, are associated with irregularities in the spin properties (Brook et al. 2016). During this period, the spin-down rate usually jumps up to a higher state (Takata et al. 2020; Shaw et al. 2022). The observed sizes of glitches coupled with emission mode switching decrease with increasing characteristic age τ_c . Notably, PSR J0738–4042 is the first pulsar that showed a significant reduction in the spin-down rate interrelated with the emergence of a new profile component, hypothesised to be caused by an asteroid encounter (Karastergiou et al. 2011; Brook et al. 2014). A large glitch with two exponential recoveries in PSR J1119–6227 was found to be coincident with the appearance of additional pulse components with intermittent or RRAT-like behaviour (Weltevrede et al. 2011). Repeated state changes have been detected in the only known variable gamma-ray pulsar PSR J2021+4026 (Takata et al. 2020). The gamma-ray pulsar PSR J1124–5916 has also experienced spin-down rate transition with no significant difference between the pulse profiles in different states (Ge et al. 2020b). The pulse profile switching between wide and narrow modes is induced by a glitch occurred in PSR B2035+36 (Kou et al. 2018). Overall, these complicated strong connections between emission and rotational properties can provide new insights into the magnetospheric conditions and neutron-star interiors.

The theoretical picture of these state-switching correlations remains ambiguous. Nevertheless, the scenario that the measurable changes in spin-down rate, flux, and pulse shape of pulsars is driven by a shift in the magnetic inclination angle α as a consequence of a glitch, has gradually become a consensus (Link & Epstein 1997; Akbal et al. 2015; Ng et al.

2016; Liu et al. 2021b). In this work, motivated by the interesting repeated mode-changing behaviours in several pulsars (Kou et al. 2018; Takata et al. 2020) and a potential for periodical variations in the emission profile and $\dot{\nu}$ of PSR J0738–4042 (Brook et al. 2014), we carry out data analysis of PSR J0738–4042 by using the combined UTMOST and Parkes timing observations conducted between March 2008 and September 2020 to keep track of the long-term rotational history and pulse profile evolution for this pulsar. Along the way a new glitch is identified associated with the pulse profile changes in PSR J0738–4042. The paper is organised as follows. Pulsar observations and data reduction methodology are outlined in Section 2. Detailed results of glitch analysis and glitch-triggered emission variations are presented in Section 3 and 4, respectively. In Section 5, the combined model of crustquake induced platelet movement and vortex creep response is applied to the observed data which enables to better explain the observed pulsar state-changing behaviour. Further discussions are made regarding these findings and their comparison with similar cases in the literature in Section 6. Finally in Section 7 the paper is closed with concluding remarks.

2 OBSERVATIONS AND ANALYSIS

PSR J0738–4042 is an isolated pulsar that was discovered 54 years ago in 1968 (Large et al. 1968), and has a spin period of $P = 374$ ms and a period derivative of $\dot{P} = 1.37 \times 10^{-15}$ (Manchester et al. 2005; Lower et al. 2020). Considering the magnetic dipole radiation as the main cause of the spin-down and if the initial spin period is much less than its current value, the spin parameters imply that this pulsar has a large characteristic age $\tau_c = P/2\dot{P} = 4320$ kyr, making it one of the oldest state-changing pulsars, with the surface magnetic field B_s and spin-down energy loss rate \dot{E} of 0.72×10^{12} G and 10×10^{32} erg/s, respectively¹ (Manchester et al. 2005; Lower et al. 2020). The mean timing noise parameter $\Delta_8 [\equiv \log(|\dot{\nu}|t^3/6\nu)]$ for PSR J0738–4042 is calculated as $-1.14(2)$ with our data, and when compared with those of 366 pulsars in Hobbs et al. (2010) indicates a high level of timing noise. This pulsar had never been reported to experience a glitch before (Brook et al. 2016).

PSR J0738–4042 has long been become a continuously tracking target at the centre frequencies of 843 MHz and 1369 MHz with the Upgraded Molonglo Observatory Synthesis Telescope (UTMOST) and Parkes 64-m Radio Telescope, respectively. All timing observations obtained for this work are publicly available from the Molonglo Online Repository² (Lower et al. 2020) and Parkes Pulsar Data Archive³ (Hobbs et al. 2011). Fig. 1 shows the distribution of the collected 12.5-yr observations ranging from MJDs 54548 (March 2008) to 59116 (September 2020) by Parkes and UTMOST in detail. Here, Parkes data have a 332 d observation gap after the measured glitch epoch so that only UTMOST data were used for determining glitch parameters. The extant UTMOST ToAs together with Parkes data have been used to analyse

¹ <https://www.atnf.csiro.au/research/pulsar/psrcat/>

² <https://github.com/Molonglo/TimingDataRelease1/>

³ <https://data.csiro.au/dap/public/atnf/pulsarSearch.zul>

Table 1. Detailed parameters for emission-rotation correlations in thirteen pulsars.

Pulsar Name (PSR)	P (s)	τ_c (kyr)	B_s (10^{12} G)	\dot{E} (10^{32} erg/s)	Glitch? (Y/N)	$\Delta\nu/\nu$ (10^{-9})	$\Delta\dot{\nu}/\dot{\nu}$ (10^{-3})	Flux?	Profile	Ref.
J0738–4042	0.3749	4320	0.727	10	N	–	–140(–)	–	$W_{50}(\uparrow)$	1
					Y	0.36(4)	3(1)	–	$W_{50}(\downarrow)$	This work
J0742–2822	0.1667	157	1.69	1400	N	–	6.6(–)	–	$W_{75}(\downarrow)$	2
					Y	102.73(11)	2.1(5)	–	*	3 - 4
J1001–5507	1.4366	441	8.71	6.9	N	–	13.0(3)	–	$W_{\text{eq}}(\downarrow)$	5
J1119–6127	0.4079	1.61	41	23000	Y	9400(300)	580(14)	–	*	6
J1543–0620	0.7090	12800	0.799	0.97	N	–	17.1(–)	–	$W_{10}(\downarrow)$	2
J1602–5100	0.8642	197	7.84	42	N	–	38.6(4)	–	$W_{10}(\uparrow)$	7 - 8
B1822–09	0.7690	233	6.42	45	N	–	24.2(4)	–	$A_{\text{pc}}/A_{\text{mp}}(\uparrow)$	2, 9
					N	–	19(1)	–	$A_{\text{pc}}/A_{\text{mp}}(\uparrow)$	2, 10
					Y	4.08(2)	0.08(1)	–	◇	11
					Y	7.2(1)	1.65(7)	–	◇	11
B1828–11	0.4050	107	4.99	360	N	–	7.1(–)	–	$W_{10}(\downarrow)$	2
J2021+4026	0.2653	76.9	3.85	1200	Y	<100(–) ^a	56(9)	$\gamma(\downarrow)$	Y	12 - 15
					N	–	31(11)	$\gamma(\downarrow)$	Y	15
B2021+51	0.5291	2740	1.29	8.2	Y	0.373(5)	–0.24(3)	–	$W_{10}(\downarrow)$	16
B2035+36	0.6187	2180	1.69	7.5	N	–	132.8(–)	–	$W_{\text{eq}}(\downarrow)$	2
					Y	7.7(8)	67(8)	–	$W_{50}(\downarrow)$	17
J2043+2740	0.0961	1200	0.354	560	N	–	59.1(–)	–	$W_{50}(\uparrow)$	2

^a: denotes that a glitch event, its size, $\Delta\nu/\nu$, is less than 10^{-7} .

^b: $A_{\text{pc}}/A_{\text{mp}}$ is the ratio of the amplitudes of the precursor and main pulse.

^c: W_{eq} is the pulse equivalent width (the ratio of the area under the pulse to the peak pulse amplitude).

^d: W_{10} , W_{50} and W_{75} are the full widths of the pulse profile at 10%, 50%, and 75% of the peak pulse amplitude, respectively.

*: represents that the appearance of additional pulse components is closely correlated with an unusual glitch.

*: indicates the correlation between the ratio of the two-components in the profile and $\Delta\dot{\nu}$, which rapidly increases after the glitch.

◇: implies the variations of the integrated mean pulse profiles in both the radio-bright (B-mode) and the radio-quiet (Q-mode) modes.

References for these parameters: 1 – Brook et al. (2014); 2 – Lyne et al. (2010); 3 – Keith et al. (2013); 4 – Dang et al. (2021); 5 – Chukwude & Buchner (2012); 6 – Weltevrede et al. (2011); 7 – Brook et al. (2016); 8 – Zhou et al. (2019); 9 – Shabanova (2007); 10 – Zou et al. (2004); 11 – Liu et al. (2022); 12 – Allafort et al. (2013); 13 – Ng et al. (2016); 14 – Zhao et al. (2017); 15 – Takata et al. (2020); 16 – Liu et al. (2021b); 17 – Kou et al. (2018).

the long-term rotational properties whereas for pulse profile variations only Parkes data have been processed. The details of the timing observations for this pulsar conducted at UT-MOST and Parkes observatory are described in Jankowski et al. (2019) and Lower et al. (2021). Meanwhile, the HartRAO ToAs recorded between MJDs 45704 (January 1984) and 54743 (October 2008) in the work of Brook et al. (2014) are obtained to revisit a previous mode-switching behaviour.

Pulsar timing techniques involve the evaluation and interpretation of the differences (also known as “timing residuals”) between the observed pulse times-of-arrival (ToAs) and predicted arrival times, which help to examine the entire rotational history of a given pulsar. In order to determine the actual ToAs, the software packages PSRCHIVE (Hotan et al. 2004) are employed in these procedures. After removing radio-frequency interference (RFI) and being de-dispersed, each observation is scrunched in time, frequency and polarisation to extract mean pulse profiles, which are subsequently aligned and added to form a standard profile template. After that the `pat` tool of PSRCHIVE is invoked to perform a cross-correlation between the observed mean profiles and the standard template to yield highly accurate ToAs of topocentric pulse. Next, these ToAs need to be transformed to the Solar system barycentre (SSB) based on the Jet Propulsion Laboratory’s (JPL) DE430 Solar-system

ephemeris (Folkner et al. 2014) and the TCB (Barycentric Coordinate Time) scale. The high-precision pulsar timing analysis software TEMPO2 (Hobbs et al. 2006) is used to obtain the timing residuals with a rotational phase model, which is introduced by a Taylor series expansion (Edwards et al. 2006):

$$\phi(t) = \phi(t_0) + \nu(t - t_0) + \frac{\dot{\nu}}{2}(t - t_0)^2 + \frac{\ddot{\nu}}{6}(t - t_0)^3 + \dots, \quad (1)$$

where ϕ , ν , $\dot{\nu}$ and $\ddot{\nu}$ are the phase, spin-frequency and its derivatives as measured at the fiducial epoch t_0 .

Conventionally, a glitch will result from an additional pulse phase modelled by the equation (Edwards et al. 2006):

$$\phi_g = \Delta\phi + \Delta\nu_p(t - t_g) + \frac{1}{2}\Delta\dot{\nu}_p(t - t_g)^2 + [1 - e^{-(t-t_g)/\tau_d}]\Delta\nu_d\tau_d, \quad (2)$$

where $\Delta\phi$ is an offset in the pulse phase at the glitch epoch t_g . The permanent increments in the pulse frequency $\Delta\nu_p$ and first frequency derivative $\Delta\dot{\nu}_p$, in addition to a transient frequency increment $\Delta\nu_d$ with an exponential decay timescale τ_d , are used to model a glitch. Hence, the observed relative glitch sizes in the rotation and the spin-down rates

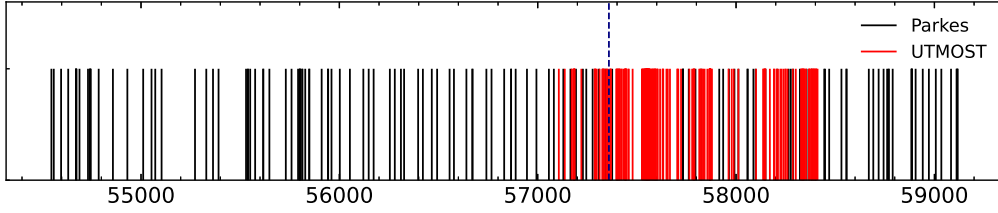


Figure 1. Distributions of Parkes (black lines) and UTMOST (red lines) observations for PSR J0738–4042. Parkes data have a 332 d observation gap after the measured glitch epoch marked by a blue dashed line.

Table 2. The fitted timing solutions and glitch parameters.

Parameter	Values
ν (Hz)	2.6672305326(2)
$\dot{\nu}$ (10^{-15} s^{-2})	−9.73(1)
Freq. epoch (MJD)	57491
TOA numbers	177
Data range (MJD)	57106–57878
Rms residual (μs)	578*/116*
Glitch epoch (MJD)	57359(5)
$\Delta\nu$ (10^{-10} Hz)	9(1)
$\Delta\nu/\nu$ (10^{-9})	0.36(4)
$\Delta\dot{\nu}$ (10^{-17} s^{-2})	−3(1)
$\Delta\dot{\nu}/\dot{\nu}$ (10^{-3})	3(1)

*: Rms before and after fitting the glitch.

are described as:

$$\frac{\Delta\nu}{\nu} = \frac{\Delta\nu_p + \Delta\nu_d}{\nu}, \quad (3)$$

$$\frac{\Delta\dot{\nu}}{\dot{\nu}} = \frac{\Delta\dot{\nu}_p - \Delta\nu_d/\tau_d}{\dot{\nu}}. \quad (4)$$

Furthermore, the parameter Q , which is defined as the ratio $\Delta\nu_d/\Delta\nu$, quantifies the fraction of glitch recovery.

3 GLITCH

In order to analyse the long-term spin behaviour of PSR J0738–4042, the weighted least-square fit is utilized to find a set of phase-connected timing solutions. The pulsar’s timing position (α , δ) referred to the result updated by Lower et al. (2020) and a constant phase offset between the UTMOST and Parkes ToAs, are included to determine a good timing model. In this process, a signature of the presence of one possible typical small glitch is identified. As is shown in panel (a) of Fig. 2, the timing residuals relative to the spin-down model before MJD $\sim 57359(5)$ are randomly distributed around zero and then show a downward trend with a parabola-like structure. To confirm if a small amplitude jump in the spin frequency has actually occurred, the time evolution of ν and $\dot{\nu}$, obtained from separate fits to a short set of overlapping observations, are displayed in panels (b) and (c) of Fig. 2. The frequency, ν , varies by $0.9(1) \times 10^{-9}$ Hz, and there is a slight decrease in the frequency derivative, $\dot{\nu}$, of $3(1) \times 10^{-17} \text{ s}^{-2}$. Apart from this, the pattern of the post-fit residuals after adding the glitch terms to the timing model in panel (d) of Fig. 2 indicates that glitch parameters

have been properly modelled. Taking all these together, a small glitch is verified to occur at MJD $\sim 57359(5)$. Glitch parameters are obtained by fitting equation (2) without the exponential decay as there is no clear evidence for this term. Because the glitch epoch cannot be determined from the TEMPO2 timing fit, it was set at the middle date of the segment between the last pre-glitch observation and the first post-glitch observation, with an uncertainty of half the observation gap. Our fitted values presented in Table 2 give $\Delta\nu/\nu = 0.36(4) \times 10^{-9}$ and $\Delta\dot{\nu}/\dot{\nu} = 3(1) \times 10^{-3}$.

Timing solutions for the pre- and post-glitch data spans are given in Table 3. These parameter values before and after the glitch are generally consistent with the ones in Brook et al. (2016) and Lower et al. (2021), respectively. We notice that this pulsar displays an apparent reversal of the sign of $\ddot{\nu}$ at the time of the glitch, with a significant difference ($\Delta\ddot{\nu} = -3.52(3) \times 10^{-24} \text{ s}^{-3}$). The underlying reason is confidently the unusual post-glitch behaviour in this pulsar, since almost all glitches display both a post-glitch value of $\ddot{\nu} \geq 0$ and a difference of $\Delta\ddot{\nu} \geq 0$ (Manchester & Hobbs 2011). In the present case, the whole 12.5-yr data set is binned into intervals of ~ 200 days to fit separately with the standard spin-down model to demonstrate in depth the evolution of $\dot{\nu}$ in panel (a) of Fig. 3. A permanent change in $\ddot{\nu}$ is confirmed with the very different slopes of $\dot{\nu}$ before and after the glitch. Clearly, this pulsar behaves in a new spin-down state after the glitch. The $|\dot{\nu}|$ steadily increases over ~ 1380 d to a peak of $10.11(1) \times 10^{-15} \text{ s}^{-2}$, and thereafter shows a decay trend. Quoting the observable ν and its first two derivatives in the two independent spin-down states from Table 3, we obtain the pre- and post-glitch braking indices ($\ddot{\nu}/\dot{\nu}^2$) $n_{\text{pre}} = 17630(580)$ and $n_{\text{post}} = -77410(880)$, the errors calculated with the linear error propagation method. Lower et al. (2021) obtained a braking index value of -96227 for PSR J0738–4042 by using a much shorter 3.6-yr UTMOST data. According to Johnston & Galloway (1999) and Alpar & Baykal (2006), a possible reason for such large braking indices is the unresolved effects of the glitches and the superfluid internal torques in the post-glitch relaxation process. Hobbs et al. (2010) and Dang et al. (2020) suggested that red timing noise should be recognized as the cause of the middle-age pulsars’ anomalously large braking indices. Yi & Zhang (2015) modeled that the fluctuation of the magnetic inclination angle α , which would correspond to a change in the effective emission geometry (Kou et al. 2018), contributes a source of red timing noise. Prior to this work Lower et al. (2020) explored the timing noise properties of the 300 UTMOST-observed radio pulsars and found that PSR J0738–4042 is the only pulsar which has been shown to

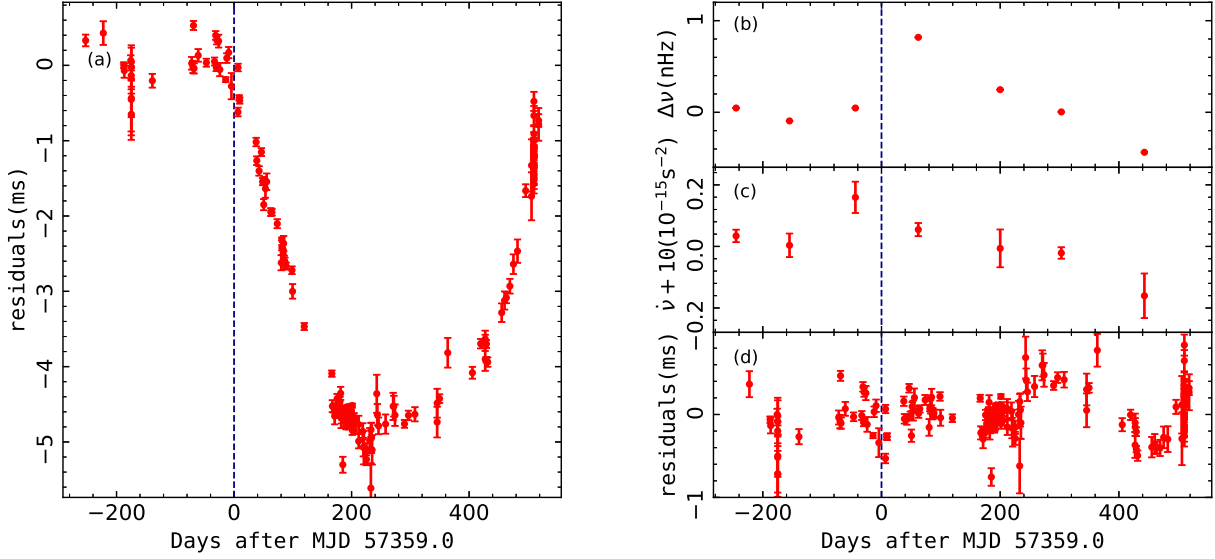


Figure 2. First glitch observed in PSR J0738–4042: (a) timing residuals with respect to the pre-glitch spin-down model; (b) variations of the frequency residuals ν after subtracting the pre-glitch spin-down model; (c) the variations of $\dot{\nu}$; (d) the post-fit residuals after adding the glitch terms listed in Table 2 to the timing model. This glitch analysis is conducted with only UTMOST data between MJDs 57106 and 57878. The vertical lines indicate the glitch epoch at MJD \sim 57359(5).

Table 3. PSR J0738–4042’s timing solutions before and after the glitch, produced by TEMPO2.

Parameter	MJD range	
	54548–57355	57363–59116
Pulsar name	PSR J0738–4042	
Right ascension, RA (J2000) (h:m:s)	07:38:32.244(3)	
Declination, DEC (J2000) (d:m:s)	–40:42:39.43(4)	
Pulse frequency, ν (Hz)	2.66723182723(3)	2.66722989447(2)
First derivative of pulse frequency, $\dot{\nu}$ (10^{-15} s^{-2})	–9.7666(4)	–9.9875(4)
Second derivative of pulse frequency, $\ddot{\nu}$ (10^{-24} s^{-3})	0.63(1)	–2.89(3)
Frequency epoch (MJD)	55951	58239
Number of ToAs	117	265
RMS timing residual (μs)	3601	2247
Dispersion measure, DM ($\text{cm}^{-3} \text{ pc}$)	160.8(6)	
Time-scale	TCB	
Solar system ephemeris model	DE430	

be in favour of the power-law red noise with $\ddot{\nu}$ (PLRN+F2) model. Alongside this, Lower et al. (2020) speculated this case could be due to not considering the state-changing behaviours in their timing noise model. These observations mean that the following analysis of the evolution of the pulse profile is an essential ingredient for characterising the true spin evolution of PSR J0738–4042.

4 PULSE PROFILE CHANGES CORRELATED WITH SPIN-DOWN CHANGES

PSR J0738–4042 underwent a switching between two- and three-components of the pulse profile since its first spin-down state transition event occurred in September 2005 (Brook et al. 2014). The triple-peaked profile of PSR

J0738–4042 contains a dominant trailing component, preceded by two obvious shoulder peaks (Brook et al. 2016). In Panels (b) and (c) of Fig. 3 we plot the pulse width at the 10 percent level of the pulse peak W_{10} and full width at half maximum of the peak W_{50} to present the evolution of the average profiles taken with the 20-cm receiver of the Parkes telescope at various times of the last 12.5-yr. Visually, the widths of both types has changed right after MJD \sim 55525, but the spin-down rates in Panel (a) of Fig. 3 are not observed to exhibit any unusual behaviour around this time. Brook et al. (2016) also reported this drastic variability in the pulse shapes. Since then, the mean pulse profiles maintain the new relatively stable state until the occurrence of this glitch, after which the profile changes get involved. It is impossible to determine whether the pulse width change

has taken place suddenly or gradually after the time of the glitch due to missing coverage of observations, but it is still clear that W_{10} increases while W_{50} decreases followed by a steady value. Table 4 provides the average pulse width measurements for each group of the observed profiles. The average W_{50} values are $18.5(4)^\circ$ before and $16.0(3)^\circ$ after the glitch. To illustrate the specific changes in the pulse profile, normalized integrated pulse profiles before and after glitch, which are derived from summing all aligned pulse profiles in MJDs 55529–57355 and MJDs 57363–59116 respectively, are plotted in panel (d) of Fig. 3. The leading peak of the post-glitch normalized profile becomes weaker, contrasting with its pre-glitch relative size, and is accompanied by an enhancement in the central component. It is worthy to note that this pulsar has a slightly wider mean pulse profile after the glitch. These concurrent changes in the average pulse profile and spin-down rate state suggest that the origin of the mode-switching phenomenon in PSR J0738–4042 is related to the glitch event.

5 THE COMBINED MODEL OF CRUSTQUAKE AND VORTEX CREEP RESPONSE FOR PULSAR GLITCHES AND PULSE SHAPE CHANGE

Vortex lines in the inner crust and core superfluids of a neutron star strongly interact with the lattice nuclei and magnetic flux tubes, respectively, and maintain the rotational equilibrium between the observed crust and interior superfluid components by thermal activation, a process called creep (Alpar et al. 1984; Gügercinoğlu & Alpar 2014). The steady-state creep process can be affected either by rotational or thermal perturbations (Cheng et al. 1988; Link & Epstein 1996). Glitches as sudden and collective vortex unpinning events temporarily stop the creep rate within the glitch affected superfluid regions and the post-glitch recovery reflects the tendency to return back to the pre-glitch conditions.

Crustquakes are invoked to explain smaller Crab-like glitches (Baym & Pines 1971; Rencoret et al. 2021) and may play a dominant role in unpinning trigger for larger glitches (Ruderman 1976; Alpar et al. 1996) since a single vortex line freed by a quake is able to release a large number of vortices in high density traps (Cheng et al. 1988; Warszawski et al. 2012). There are three main contributions to strain in the crust that generate a fracturing quake: a combination of gravitational force and centrifugal force with secular spin-down (Giliberti et al. 2020; Rencoret et al. 2021) or crustal magnetic field (Franco et al. 2000; Lander et al. 2015) or pinning stress due to vortex-nuclei interaction (Ruderman 1976; Anderson et al. 1982) and vortex-flux tube entanglement at the base of the crust (Ruderman et al. 1998; Sedrakian & Cordes 1999). The spin-down induced stresses act to reduce the centrifugal bulge of the neutron star crust formed when the star was rotating much faster. Thus, after experiencing successive glitches the neutron star assumes a spherical shape which limits the extent of the crustquakes via spin-down. Given the surface magnetic field strength estimate from the dipole formula is $B_d = 7.27 \times 10^{11}$ G for PSR J0738–4042, the crustal magnetic field originated stresses are not expected to play an important role in quakes. Since both the spin-down and crustal magnetic field induced

stresses are in the direction of the magnetic pole, their contributions will be to decrease inclination angle after a quake (Lander et al. 2015).

The stresses associated with vortex line-flux tube pinning at the base of the crust, on the other hand, is in the direction of the neutron star equator (Ruderman et al. 1998; Gügercinoğlu & Alpar 2016). Whenever this continuous growth rate of the stress approaches the yielding point a crust breaking quake takes place and leads broken platelet to displace. The event may induce inward superfluid vortex line motion towards the rotational axis and in turn initiate collective vortex unpinning, thus playing the role of glitch trigger. Since the footpoints of global magnetospheric field lines are anchored in the crust, any irreversible motion of the broken platelet will be accompanied by tiny growth in the inclination angle between the rotation and magnetic dipole moment axes. Another influence of the platelet movement will be the small scale increase of the curvature of the local magnetic field lines in the vicinity of the polar cap, a process that may cause emission changes. The changes in the radio emission arise from the modifications of the surface magnetic field in the inner magnetospheric region above the polar cap (Geppert et al. 2021). Here is the place where radio emission originates through electron/positron pairs formation and acceleration in a sufficiently strong and curved field ensues. Since the outer gap regions wherein X-ray and gamma radiation presumably occur are located well above the polar cap, it is more difficult to observe pulse profile variations in these short wavelengths concurrent with the glitch event.

The pulse width at half maximum W_{50} is related to the pulse period P and the inclination angle α via (Rankin 1990; Maciesiak & Gil 2011)

$$W_{50} = 2^\circ.45 \frac{P^{-1/2}}{\sin \alpha}. \quad (5)$$

A similar fit formula applied to a larger sample of radio pulsars exists for W_{10} values (Posselt et al. 2021)

$$W_{10} = (11.9 \pm 0.4)^\circ (P/\text{s})^{-0.63 \pm 0.06}. \quad (6)$$

The mean W_{50} values in Table 4 for the pulse width measurements before and after the 2015 glitch event yield, by using equation (5), the inclination angles $12^\circ.5$ and $14^\circ.6$ respectively, before and after the glitch of PSR J0738–4042. Therefore, the increment of $\Delta\alpha = 2^\circ.1$ in the inclination angle seems to be produced by the glitch event itself. However, W_{10} value predicted by equation (6) ($20^\circ - 24^\circ$) differs significantly from the observed $W_{10} \approx 35^\circ$, indicating that newly emerged component affected the pulse profile largely.

In the plasma filled magnetosphere inclination angle evolution under the the central dipole radiation approximation leads to the following equation which is constant throughout the lifetime of a pulsar (Philippov et al. 2014; Ekşi et al. 2016)

$$C \equiv \frac{\cos^2 \alpha_0}{P_0 \sin \alpha_0} = \frac{\cos^2 \alpha}{P \sin \alpha}, \quad (7)$$

where the subscript ‘0’ refers to the measurement of the corresponding quantity at a particular time. The plasma magneto-hydrodynamics pulsar alignment time-scale for PSR J0738–4042 is $\tau_{\text{align}}^{MHD} = \tau_c \sin^2 \alpha_0 / \cos^4 \alpha_0 = 0.3$ Myr which means that pulsar will evolve toward alignment on a

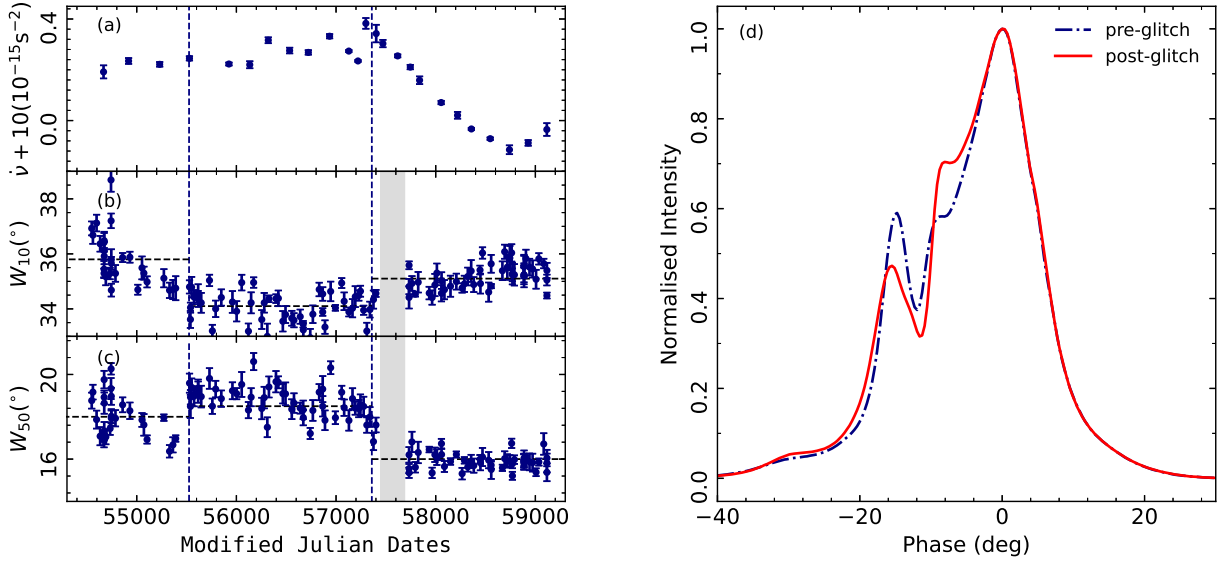


Figure 3. Emission-rotation correlation in PSR J0738–4042: (a) long-term evolution for the spin-down rate $\dot{\nu}$ obtained from the combined UTMOST and Parkes data; (b) and (c) the pulse width W_{10} and W_{50} at 10% and 50% of the peak for all 1369-MHz integrated pulse profiles observed at Parkes, respectively; (d) the integrated normalized pulse profiles at pre- (blue line) and post-glitch (red line) modes. Grey areas in panels (b) and (c) signify the observation gap between MJDs 57400 and 57732 of Parkes data. The two vertical lines mark the epoch at MJD \sim 55525 and the first glitch occurred at MJD \sim 57359(5). The horizontal lines are stand for the average values of W_{10} and W_{50} (listed in Table 4) at three different modes.

Table 4. Pulse widths W_{10} and W_{50} in three different spin-down states.

Parameter	Pre-glitch	Pre-glitch	Post-glitch
Data span (MJD)	54548–55391	55529–57355	57363–59116
Mean $W_{10}(\text{°})$	35.8(2)	34.1(2)	35.1(2)
Mean $W_{50}(\text{°})$	18.0(3)	18.5(4)	16.0(3)
Number of pulse profiles	23	54	51

long time-scale provided that its evolution is not interrupted by other timing events.

Another effect of the crust breaking event on the pulsar dynamics would be its imprints on the rotational evolution. Crust breaking may be an agent for variation of the steady-state vortex current in the inner crust of neutron stars, in particular play an important role in glitches by transporting some of the vortices inward and unpinning the others. This model was successfully applied to the timing behaviours of PSR J1119–6127 (Akbal et al. 2015) and the Crab pulsar (Gügercinoğlu & Alpar 2019). Our model for the post-glitch spin-down rate evolution is (Gügercinoğlu & Alpar 2019)

$$\Delta\dot{\nu}(t) = -\frac{I_{A'}}{I} |\dot{\nu}_{\infty}| \left[1 - \frac{1}{1 + (e^{-t_0/\tau_{n1}} - 1) e^{-t/\tau_{n1}}} \right] - \frac{I_A}{I} |\dot{\nu}_{\infty}| \left[1 - \frac{1}{1 + (e^{t_0/\tau_{n1}} - 1) e^{-t/\tau_{n1}}} \right], \quad (8)$$

where $\dot{\nu}_{\infty}$ is the spin-down rate just before the glitch, I_A/I , t_0 , τ_{n1} are nonlinear superfluid region’s fractional moment of inertia, offset time, and recoupling time-scale for outward moving vortex lines at the time of glitch and primed quanti-

ties are their inward moving vortices counterparts. The nonlinear creep regions are responsible for glitches since through these regions conditions are very close to lead to vortex unpinning avalanche. The post-glitch response of these nonlinear regions are determined by two timescales: recoupling time-scale τ_{n1} is the time for coupling of the glitch affected nonlinear superfluid region to the other superfluid components of the star. The offset time t_0 determines the time-scale on which glitch affected decrease in the angular velocity lag between the superfluid and crustal rotational rates turns back towards the original pre-glitch value again by the neutron star spin-down. Note that if equal number of vortex lines move inward and outward after the collective unpinning event and traverse the same radial extent, then glitch magnitude in the spin frequency will be tiny or even zero. However, due to the time variation of the interior superfluid torque acting on the neutron star, the spin-down rate will first experience a gradual slow increase, i.e. become more negative, as a result of inward motion of vortices, and after a certain time it will reverse and start to decay toward the original pre-glitch value as outward moving vortex lines repin and restart creep again.

Table 5. Inferred vortex creep model parameters for the fit to PSR J0738–4042 post-glitch timing data. Here we have used the standard notation that $(A)_a = A \times 10^a$.

Parameter	Value
$\left(\frac{I_{A'}}{I}\right)_{-2}$	1.9(2)
$\left(\frac{I_A}{I}\right)_{-2}$	4.9(6)
$\left(\frac{I_B}{I}\right)_{-2}$	1.6(7)
t'_0 (days)	41238(4578)
t_0 (days)	1868(310)
τ'_{nl} (days)	19600(1902)
τ_{nl} (days)	211(19)
$\delta\Omega'_s$ (rad s ⁻¹) ₋₆	37.5(5.0)
$\delta\Omega_s$ (rad s ⁻¹) ₋₆	1.7(3)

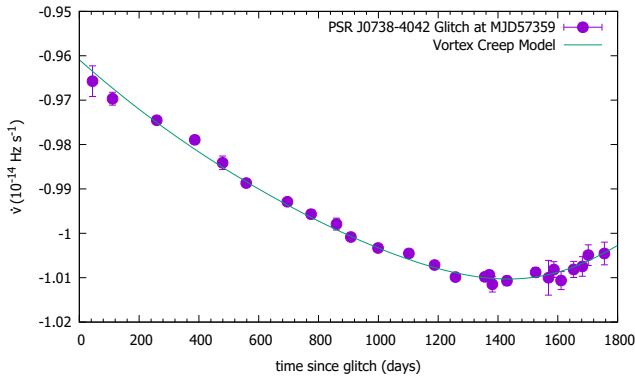


Figure 4. Comparison between the glitch occurred at MJD 57359 (purple) and the vortex creep model prediction (green).

We apply equation (8) to the post-glitch recovery of 2015 event. Comparison between the vortex creep model and the 2015 glitch data is displayed in Fig. 4. Best fit model parameters are shown in Table 5.

Given that non-linear superfluid relaxation time-scale is $\tau'_{\text{nl}} \approx 50$ yr, the spin-down rate fluctuations before the glitch can be understood as time variable superfluid coupling to the external pulsar braking torque (Gügercinoglu & Alpar 2017). Note that damped sinusoidal-like oscillations had also been observed before and after the 1988 Christmas glitch of the Vela pulsar (McCulloch et al. 1990) and second largest ever glitch in PSR B2334+61 (Yuan et al. 2010b). The fractional moment of inertia of the non-linear creep regions participated to PSR J0738–4042 glitch is similar to those of Vela-like pulsars (Gügercinoglu et al. 2022b), in line with the expectation that older pulsars have well-established vortex trap network (Alpar & Baykal 2006). The total number of vortices involved in the 2015 glitch can be estimated as

$$N_v = \frac{2\pi R^2 (\delta\Omega_s + \delta\Omega'_s)}{\kappa} = 5.43 \times 10^5 \frac{(t_0 + t'_0)|\dot{\nu}_\infty| R^2}{\kappa}, \quad (9)$$

with $\kappa = 2 \times 10^{-3} \text{ cm}^2 \text{ s}^{-1}$ being the quantized vorticity attached to each vortex line and R being the neutron star radius and the change in the superfluid angular velocity $\delta\Omega_s$ due to vortex discharge is related to offset

time t_0 with $\delta\Omega_s = 2\pi|\dot{\nu}|t_0$. Numerical values in Table 5 gives $N_v = 3.57 \times 10^{10}$ which is three orders of magnitude smaller than the values inferred for larger glitches in the Crab (Gügercinoglu & Alpar 2019), Vela (Akbal et al. 2017; Gügercinoglu & Alpar 2020), and PSR J1119–6127 (Akbal et al. 2015). The total fractional crustal superfluid moment of inertia included in the 2015 glitch of PSR J0738–4042 from Table 5 is $I_{\text{cs}}/I = (I_A + I_{A'} + I_B)/I = (8.4 \pm 0.9) \times 10^{-2}$, which puts a lower bound on the crustal moment of inertia and in turn implies a stiff equation of state for neutron star matter. Here I_B is the capacitive vortex traps in which vortices do not creep at all and obtained from the angular momentum balance during the glitch [see, for instance, Equation (12) in (Akbal et al. 2015)]. This I_{cs} is consistent with the fact that neutron stars should have a large crust to deposit substantial amount of angular momentum which will be tapped at giant glitches (Delsate et al. 2016; Shang & Li 2021).

The total crustal superfluid moment of inertia involved in the 2015 glitch I_{cs} can be used to put a constraint on the surface temperature of PSR J0738–4042. For older pulsars in which the original heat content had been radiated away via neutrino emission and photons from the surface, the residual heat arising from the superfluid friction implies a surface temperature (Alpar et al. 1984)

$$T_s = \left(\frac{I_{\text{cs}} \bar{\omega}_{\text{cr}} |\dot{\Omega}|}{4\pi\sigma R^2} \right)^{1/4}, \quad (10)$$

where $\bar{\omega}_{\text{cr}}$ is the value of the critical angular velocity between the inner crust superfluid and the normal matter before vortex line unpinning that averaged over the pinning layers, $|\dot{\Omega}| = 2\pi|\dot{\nu}|$ is the magnitude of the first time derivative of the pulsar angular velocity, σ is the Stefan-Boltzmann constant, $R \cong 10^6$ cm is the neutron star radius. Since there are other heating mechanisms for older pulsars, like rotochemical heating (González-Jiménez et al. 2015) and dissipation due to vortex line-flux tube interaction (Sedrakian & Sedrakian 1993), equation (10) provides a lower limit to the surface temperature of PSR J0738–4042. By taking $\bar{\omega}_{\text{cr}} = 3.9 \times 10^{-2} \text{ rad s}^{-1}$ from Table 6 we obtain the estimate $T_s = 1.38 \times 10^5$ K. Future spectral observations of PSR J0738–4042 will reveal the surface blackbody temperature of this middle-aged pulsar.

From the non-linear superfluid recoupling time-scales τ'_{nl} and τ_{nl} ,

$$\tau'_{\text{nl}}, \tau_{\text{nl}} = \frac{kT \omega_{\text{cr}}}{E_p |\dot{\Omega}|}, \quad (11)$$

with E_p being the pinning energy per vortex line-nucleus intersection and k being the Boltzmann constant, one can estimate the location of the glitch trigger for collective unpinning event. Since the ratio ω_{cr}/E_p depends uniquely on the density of the neutron star crust, for a given microscopic neutron star model τ_{nl} found from fits helps to constrain the density (location) which is responsible for the glitch trigger. We employ SLy4 equation of state for $1.4M_\odot$ neutron star (Douchin & Haensel 2001) and use Gudmundsson et al. (1983) formula $T_8 = 1.288(T_{\text{s}6}^4/g_{\text{s}14})^{0.455}$ to convert neutron star surface temperature T_s from the estimate given in equation (10) to internal temperature T . Here we define $Q_x = Q/10^x$ for the corresponding quantity Q in cgs units. For the chosen neutron star model the gravitational redshift

Table 6. Vortex line-nucleus pinning related microphysical parameters and nonlinear recoupling time-scale estimates for five crustal layers. Entries in the first three columns are taken from [Seveso et al. \(2016\)](#) ($\beta = 3$ model). The last column is calculated from equation (11).

ρ (10^{13} g cm $^{-3}$)	E_p (MeV)	ω_{cr} (10^{-2} rad s $^{-1}$)	τ_{nl} (days)
0.15	0.17	9.45	24125
0.96	0.24	1.44	2612
3.4	2.08	11.4	2373
7.8	0.69	10.8	678
13	0.02	0.02	463

corrected surface gravity is $g_{s14} = 1.78$. The non-linear superfluid recoupling time-scales calculated by equation (11) for the five distinct pinning layers in the inner crust are displayed in the last column of Table 6. The non-linear superfluid recoupling time-scale decreases monotonically with increasing density throughout the inner crust. An inspection of Tables 5 and 6 reveals that the vortex inward motion has started from a superfluid layer just beneath of the neutron star outer crust close to the neutron drip point (in connection with the fit result $\tau'_{nl} = 19600 \pm 1902$ days) and the vortex unpinning avalanche extended to the densest pinning layer in the vicinity of the crust-core interface (in connection with the fit result $\tau_{nl} = 211 \pm 19$ days). These findings support our scenario that glitch in PSR J0738–4042 has occurred as a result of crustquake induced vortex unpinning avalanche and involved the whole crustal superfluid. The smallness of the glitch magnitude is due to the low number of vortex lines participated to the event.

The $I_{A'}/I$ value obtained from the post-glitch timing fits can be used to determine the size of the broken platelet. If one assumes a neutron star model in which a thin crust is floating above an incompressible core, $I_{A'}/I$ is related to the broken platelet size as ([Akbal et al. 2015](#); [Gügercinoğlu & Alpar 2019](#))

$$\frac{I_{A'}}{I} \cong \frac{15}{2} \frac{D}{R} \sin \alpha \cos^2 \alpha. \quad (12)$$

By using $I_{A'}/I \cong 1.9 \times 10^{-2}$ from Table 5 and $\alpha = 12^\circ.5$ corresponding to W_{50} value in Table 4 we obtain $D \approx 6 \times 10^{-4} R = 6$ m for the platelet size of PSR J0738–4042. This platelet size is similar to the $D = (5.7 - 18.1)$ m value deduced for the largest glitch in the young Crab pulsar ([Gügercinoğlu & Alpar 2019](#)), indicating a universal global pulsar quantity which depends on the neutron star matter properties and the critical strain angle.

We have also applied our model equation (8) to the 2007 timing event observed by [Brook et al. \(2014\)](#). This timing event was preceded by the state transition in the spin-down

Table 7. Inferred vortex creep model parameters for the fit to 2007 timing event observed in PSR J0738–4042.

Parameter	Value
$\left(\frac{I_{A'}}{I}\right)_{-2}$	0.65(16)
$\left(\frac{I_A}{I}\right)_{-2}$	13.7(1.3)
t'_0 (days)	2290(1150)
t_0 (days)	400(12)
τ'_{nl} (days)	1003(662)
τ_{nl} (days)	78(10)
$\delta\Omega'_s$ (rad s $^{-1}$) $_{-6}$	1.95(98)
$\delta\Omega_s$ (rad s $^{-1}$) $_{-6}$	0.34(1)
t_{th} (days)	634(41)
t_{obs} (days)	667

rate as shown in Fig. 5. The behaviour is reminiscent of the vortex line reconfiguration inside the neutron star just like the case of the 2015 glitch. The fit result is shown in Fig. 6 and the inferred model parameters are given in Table 7. Theoretical expectation of the duration of the event due to the time variable perturbed interior superfluid coupling with the pulsar braking is $t_{th} = t_0 + 3\tau_{nl} = 634(41)$ days and matches quite well with the observed time-scale $t_{obs} = 667$ days. The implied radial extent traversed by the unpinned vortices as well as their numbers is slightly larger in this case, presumably due to the involvement of some lines in the core superfluid by thermo-rotational instability. See section 6 for details.

6 DISCUSSION

In December 2015 (MJD ~ 57359), PSR J0738–4042 has experienced a spin frequency jump of magnitude $9(1) \times 10^{-10}$ Hz, that is reported as its first glitch. The discovery of this small glitch, with measured values $\Delta\nu/\nu = 0.36(4) \times 10^{-9}$ and $\Delta\dot{\nu}/\dot{\nu} = 3(1) \times 10^{-3}$, is a serendipitous result of searching for new variations in the emission profile and $\dot{\nu}$ of this pulsar with the released UTMOST and Parkes timing datasets. This glitch is in the expected size range of the UTMOST undetected events, which was set to $4.1 \times 10^{-11} - 2.7 \times 10^{-7}$ based on injection studies performed by [Dunn et al. \(2022\)](#). According to the multiple statistical studies of the glitch behaviours (see, e.g., [Dang et al. \(2020\)](#); [Basu et al. \(2022\)](#)), a striking aspect is that the observed event sizes of pulsars with large τ_c show a clear trend towards being smaller. For old pulsars with $\tau_c > 1$ Myr, $\Delta\nu/\nu$ of almost all glitches are smaller than 10^{-7} ([Liu et al. 2021b](#)) and their occurrence rate is much lower than that of young pulsars ([Dang et al. 2020](#)). Indeed, PSR J0738–4042 is a relatively old pulsar with $\tau_c > 4$ Myr but underwent only a small glitch in its ~ 48 -yr of rotational history ([Manchester et al. 1983](#); [Downs & Reichley 1983](#); [Cordes & Downs 1985](#); [Downs & Krause-Polstorff 1986](#); [Brook et al. 2014](#)). To quantify a pulsar’s glitching rate, [McKenna & Lyne \(1990\)](#) introduced the glitch activity parameter A_g , which is defined as $\frac{1}{T} \sum \frac{\Delta\nu}{\nu}$, where T is the total time searched for spin-up events. Compared with glitching pulsars of similar age ([Dang](#)

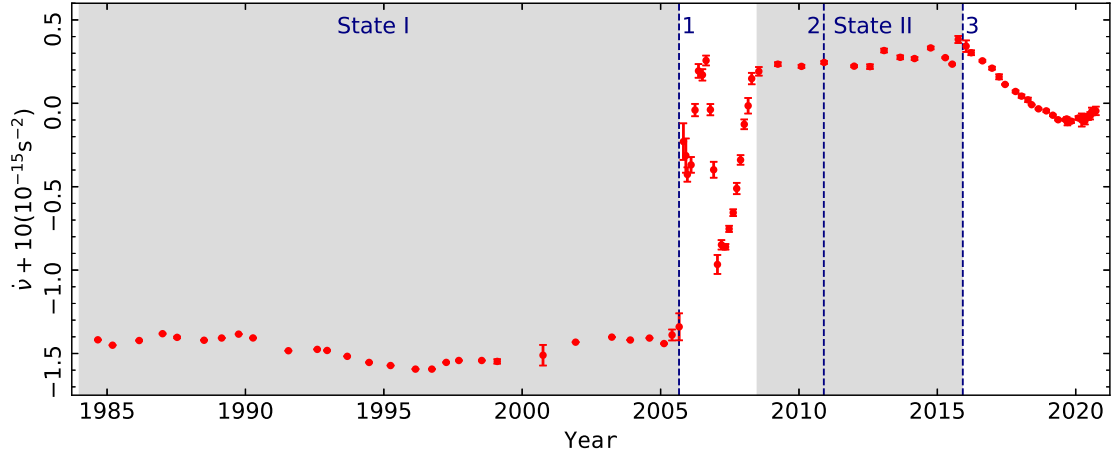


Figure 5. The 37-year evolution of the spin-down rate for PSR J0738–4042. Two grey areas indicate the high spin-down rate State I ($|\dot{\nu}|_{\text{high}} \sim -11.45 \times 10^{-15} \text{ s}^{-2}$) and the low spin-down rate State II ($|\dot{\nu}|_{\text{low}} \sim -9.76 \times 10^{-15} \text{ s}^{-2}$). The vertical dashed lines 1 and 2 indicate the epochs of the pulse profile transitions in September 2005 (MJD ~ 53614) and November 2010 (MJD ~ 55525), respectively, and line 3 is the time that new profile shape changes are associated with a glitch occurred in December 2015 (MJD ~ 57359).

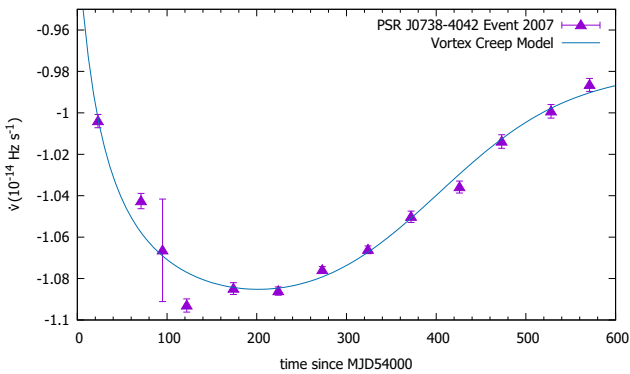


Figure 6. Comparison between the timing event occurred at MJD 54000 (purple triangles) and the vortex creep model prediction (blue).

et al. 2020), PSR J0738–4042 shows a clearly low value of $A_g \sim 7.5(8) \times 10^{-12} \text{ yr}^{-1}$.

The spin-down rate of PSR J0738–4042 exhibited only a transient small increase at the time of the glitch. The possibility of the existence of an exponential recovery with $\tau_d \geq 9$ days can be safely ruled out, because the data interval around the glitch is less than this timescale. Such behaviours are similar to the other typical small glitches observed to date. Another crucial point for PSR J0738–4042 is that, unlike almost all other normal glitches, the post-glitch relaxation has an abnormal $|\dot{\nu}|$ evolution. It is also possible to have large spin-down rate variations for pulsars by magnetospheric charge deviation from the Goldreich-Julian density (Shaw et al. 2022), asteroid encounter (Brook et al. 2014; Yu & Huang 2016) and internal superfluid modes due to vortex bending (Güercinoğlu et al. 2022a) apart from glitches. More specifically, the post-glitch spin-down rate $|\dot{\nu}|$ continues to increase with a parabolic-like tendency. As shown in

panel (a) of Fig. 3, the post-glitch $|\dot{\nu}|$ is about 5.1(2)% larger than the pre-glitch value, until the turnover point is reached at around MJD 58740 (September 14, 2019). Similar post-glitch features have been seen in some unusual glitches, and can not be understood directly by the standard glitch models. Manchester & Hobbs (2011) detected the largest glitch ever recorded ($\Delta\nu/\nu \sim 33250 \times 10^{-9}$) in PSR J1718–3718, with the post-glitch upward trend in $|\dot{\nu}|$ continued over two years. A delayed spin-up of spin frequency in the Crab pulsar during its largest glitch is related with a rapid increase in $|\dot{\nu}|$ (Shaw et al. 2018; Ge et al. 2020a). The transition between the dual spin-down states together with the steady increase in $|\dot{\nu}|$ of PSR J1001–5507 is accompanied by pulse shape variations (Chukwude & Buchner 2012), establishing a firm correlation.

Herein, 37-yr evolution of the spin-down rate $|\dot{\nu}|$ for PSR J0738–4042 between 1984 and 2021 is revisited and presented in Fig. 5. This pulsar displays mainly two distinct stable spin-down rate (State I: $|\dot{\nu}|_{\text{high}} \sim -11.45 \times 10^{-15} \text{ s}^{-2}$ and State II: $|\dot{\nu}|_{\text{low}} \sim -9.76 \times 10^{-15} \text{ s}^{-2}$). The ratio of duration in the State I and State II is $\sim 60\%$ and $\sim 20\%$, respectively. The rest of the time pulse profile changes are spotted with complex transitions in the spin-down rate. Brook et al. (2014) linked the unexpected presence of a new profile component to the drastic change in its spin-down rate beginning in 2005. One decade after the first case, this pulsar repeated the spin-down rate state change with integrated profile shape variations. Nonetheless, these two mode-switching events display some distinguishing features. The former shows the crucial change on the leading edge whereas the latter presents the leading component recession, accompanied by an obvious enhancement of the middle part of the pulse profile. The fractional amplitude of the spin-down rate change in 2005 event is more than twice that of the recently observed one. Moreover, the peculiar emission properties in 2015 event are associated with a glitch.

There are at least two possible reasons, one internal and

one external origin, which can be responsible for the transition from high spin-down rate State I to the low spin-down rate State II for PSR J0738–4042 around 2005 September. According to the internal scenario, a thermal runaway will lead to an increase in the radial vortex creep rate. Standard cooling calculations (Yakovlev & Pethick 2004; Page et al. 2006) predict that a 1 Myr-old neutron star should have a surface temperature well below 10^5 K if no heating processes are present. However, vortex creep against lattice nuclei in the inner crust (Alpar et al. 1984) and magnetic flux tubes in the outer core (Gügercinoglu 2017) give rise to superfluid friction with normal matter which dissipates rotational energy and heats up the neutron star interior. The resulting interior temperature rise will change the coupling between the interior superfluid components and the observed crust which leads to a thermo-rotational instability (Greenstein 1979) by which a substantial decrease in the magnitude of the spin-down rate may occur. The resulting excess creep rate may also unpin vortex lines in the outer core as angular velocity lag here is closer to the critical threshold for catastrophic unpinning conditions (Gügercinoglu & Alpar 2016). This may also account for the 2007 timing event. As for the external origin case, a debris disk and asteroid belt may form around neutron stars from supernova fallback matter. The tidal disruption and evaporation of asteroid matter by pulsar gravitational field and irradiation, and their interaction with the magnetosphere may also lead spin-down rate transitions. Brook et al. (2014) considered the effect of injected charged density on the activation of pair production regions in the magnetospheric gap regions. The pollution of accelerator gaps reduces the braking torque on the pulsar and in turn gives rise to a low spin-down rate. Yu & Huang (2016), on the other hand, have taken angular momentum transfer from the debris disk onto the surface of the neutron star into account as the main cause of reduction in the spin-down rate of PSR J0738–4042.

Identifying new concurrent variations in pulse profile and timing behaviours makes PSR J0738–4042 the seventh glitch-driven state-switching pulsar. Of the mode-switching pulsars in Table 1, the rotational and other properties of PSR B2021+51 are most comparable with PSR J0738–4042, especially the characteristic age. Liu et al. (2021b) revealed that the presence of emission state switching phenomenon in PSR B2021+51 manifests itself in wider mean pulse profiles following a small glitch with $\Delta\nu/\nu = 0.373(5) \times 10^{-9}$. In addition, the post-glitch spin-down rate first gradually increased and after a definite time it reversed and started to decay. These features are just like the case of PSR J0738–4042. Liu et al. (2021b) argued that the changes of the integrated profile are a manifestation of the movements of flux tubes in the emission zone during the glitch. According to the scenario presented in this paper, the spin-down rate shown in the bottom panel of Figure 2 of Liu et al. (2021b) can be fully explainable in terms of the combined vortex creep response of the inward and outward moving vortices during glitch. The fact that its W_{50} pulse width experienced an increment after the glitch is a consequence of the spin-down rate induced quake instead. Another remarkable case discovered in PSR B2035+36 has been explained as a shift in the magnetic inclination angle α due to the occurrence of a glitch (Kou et al. 2018). Meanwhile, Kou et al. (2018) also speculated that glitch may change the out-

flowing particle density in the magnetosphere, leading to a persistent increasing spin-down rate. Although all previous studies considered that these state-switching behaviours are induced by the glitch event, no in-depth analysis based on the mechanism behind glitch has been performed, to interpret these simultaneous variations in profile shape and $\dot{\nu}$. In the superfluid picture, the persistent increase of the spin-down rate following the glitch of PSR B2035+36 can be elucidated in terms of the formation of a new vortex trap at the time of the glitch wherein the vortex current has ceased.

7 CONCLUSIONS

In this work we present the identification of a repeated emission-rotation correlation occurred in PSR J0738–4042, by analysing the combined UTMOST and Parkes data. The newly discovered glitch followed by a sustained increase in the spin-down rate over 1380 d is considered to correlate with variations in the shape of the integrated pulse profile. This event is very important to establish interrelation between the magnetospheric processes and the neutron-star internal dynamics. We evaluate the 2015 pulse profile change-spin-down rate variation correlation as being a consequence of the crustquake induced inclination change and vortex line movement. The irreversible displacement of the broken crustal platelet in the direction of the neutron star equator has brought about a tiny increment in the pulsar obliquity which resulted in the narrowing of the pulse profile as is evident from comparison of W_{50} pulse width values before and after of the event. Shift of the platelet also carried vortices attached on it. The associated change of the vortex line configuration was resulted in gradual increase of the spin-down rate which survived on very long time-scale. This scenario enabled us to infer neutron star parameters like the moment of the inertia and recoupling time-scale of the crustal superfluid. Our results given in Table 5 means that PSR J0738–4042 should have a thick crust and in turn stiff equation of state. We estimated the total number of vortices that involved in the glitch event. The number of vortices is thousand times smaller than inferred for the large glitches experienced by the Vela-like pulsars. We conclude that for PSR J0738–4042 either the typical distance between the vortex traps are large and has an unconnected vortex network or the low temperature of its crust reduces the vortex-vortex scattering rate which is responsible for large-scale unpinning avalanche. We put a lower limit to the surface temperature of this pulsar by invoking superfluid friction with normal matter. We also estimated the size of the broken platelet which seems to be a global pulsar quantity reflecting the magnitude of the critical strain angle of neutron star crystal.

The model we propose has a predictive feature: if the spin-down rate variation is a consequence of the combined inward and outward motion vortex lines during a crust breaking quake, it will first display a gradual increase and start to decay after a certain time determined by the superfluid recoupling time-scale affected by the glitch. The pulse profile would become wider (narrower) if the underlying physical mechanism for broken platelet motion during the glitch was a crustquake arising from spin-down (vortex line-flux tube pinning) stresses. The ongoing monitoring

of PSR J0738–4042 at multiple radio wavelengths will certainly be a pragmatic approach to investigate the relationships between the concurrent changes in the pulse shape and timing behaviours, and help to discriminate among different models proposed for mode-switching behaviours discovered in 2005.

ACKNOWLEDGEMENTS

The Parkes radio telescope is part of the Australia Telescope, which is funded by the Commonwealth of Australia for operation as a National Facility managed by the Commonwealth Scientific and Industrial Research Organisation (CSIRO). The Molonglo Observatory is owned and operated by the University of Sydney. Major support for the UTMOST project has been provided by Swinburne University of Technology. Our work is funded by the National Natural Science Foundation of China via NSFC-11373064, 11521303, 11733010, 11873103, U2031121, 11873080, 12105231, U1838201, U1838202, U1838104, U1938103, U1938109, U1731111, U1938117, 11988101, U1731238, and 11703003. S.Q.Z. is also supported by the Sichuan Youth Science and Technology Innovation Research Team (No. 21CXTD0038) and the Fundamental Research Funds of China West Normal University (No. 20B009). Z.W.F. acknowledges support from the Guiding Local Science and Technology Development Projects by the Central Government of China no. 2021ZYD0031. We are thankful to Professor Simon Johnston for kindly sharing the data in Brook et al. (2014) with us. We would like to express our gratitude to everyone who contributed to make this study possible. We appreciate the referee for insightful comments which led to clarify the presentation.

DATA AVAILABILITY

The data used to produce figures in this article will be shared upon request to the authors.

REFERENCES

- Akbal O., Gügercinoğlu E., Şaşmaz Muş S., Alpar M. A., 2015, *MNRAS*, **449**, 933
- Akbal O., Alpar M. A., Buchner S., Pines D., 2017, *MNRAS*, **469**, 4183
- Allafort A., et al., 2013, *ApJ*, **777**, L2
- Alpar M. A., Baykal A., 2006, *MNRAS*, **372**, 489
- Alpar M. A., Anderson P. W., Pines D., Shaham J., 1984, *ApJ*, **276**, 325
- Alpar M. A., Chau H. F., Cheng K. S., Pines D., 1996, *ApJ*, **459**, 706
- Anderson P. W., Alpar M. A., Pines D., Shaham J., 1982, *Philosophical Magazine, Part A*, **45**, 227
- Arzoumanian Z., Nice D. J., Taylor J. H., Thorsett S. E., 1994, *ApJ*, **422**, 671
- Ashton G., Lasky P. D., Graber V., Palfreyman J., 2019, *Nature Astronomy*, **3**, 1143
- Basu A., et al., 2022, *MNRAS*, **510**, 4049
- Baym G., Pines D., 1971, *Annals of Physics*, **66**, 816
- Boynon P. E., Groth E. J., Hutchinson D. P., Nanos G. P. J., Partridge R. B., Wilkinson D. T., 1972, *ApJ*, **175**, 217
- Brook P. R., Karastergiou A., Buchner S., Roberts S. J., Keith M. J., Johnston S., Shannon R. M., 2014, *ApJ*, **780**, L31
- Brook P. R., Karastergiou A., Johnston S., Kerr M., Shannon R. M., Roberts S. J., 2016, *MNRAS*, **456**, 1374
- Cheng K. S., 1987, *ApJ*, **321**, 805
- Cheng K. S., Alpar M. A., Pines D., Shaham J., 1988, *ApJ*, **330**, 835
- Chukwude A. E., Buchner S., 2012, *ApJ*, **745**, 40
- Cordes J. M., Downs G. S., 1985, *ApJS*, **59**, 343
- Dang S. J., et al., 2020, *ApJ*, **896**, 140
- Dang S. J., et al., 2021, *RAA*, **21**, 042
- Delsate T., Chamel N., Gürlebeck N., Fantina A. F., Pearson J. M., Ducoin C., 2016, *Phys. Rev. D*, **94**, 023008
- Dib R., Kaspi V. M., 2014, *ApJ*, **784**, 37
- Douchin F., Haensel P., 2001, *A&A*, **380**, 151
- Downs G. S., Krause-Polstorff J., 1986, *ApJS*, **62**, 81
- Downs G. S., Reichley P. E., 1983, *ApJS*, **53**, 169
- Dunn L., et al., 2022, *MNRAS*, **512**, 1469
- Edwards R. T., Hobbs G. B., Manchester R. N., 2006, *MNRAS*, **372**, 1549
- Ekşi K. Y., Andaç I. C., Çıkıntoğlu S., Gügercinoğlu E., Vahdat Motlagh A., Kızıltan B., 2016, *ApJ*, **823**, 34
- Espinoza C. M., Lyne A. G., Stappers B. W., Kramer M., 2011, *MNRAS*, **414**, 1679
- Folkner W. M., Williams J. G., Boggs D. H., Park R. S., Kuchynka P., 2014, *Interplanetary Network Progress Report*, **42-196**, 1
- Franco L. M., Link B., Epstein R. I., 2000, *ApJ*, **543**, 987
- Ge M. Y., et al., 2020a, *ApJ*, **896**, 55
- Ge M. Y., et al., 2020b, *ApJ*, **900**, L7
- Geppert U., Basu R., Mitra D., Melikidze G. I., Szkudlarek M., 2021, *MNRAS*, **504**, 5741
- Giliberti E., Cambiotti G., Antonelli M., Pizzochero P. M., 2020, *MNRAS*, **491**, 1064
- González-Jiménez N., Petrovich C., Reisenegger A., 2015, *MNRAS*, **447**, 2073
- Greenstein G., 1979, *Nature*, **277**, 521
- Gudmundsson E. H., Pethick C. J., Epstein R. I., 1983, *ApJ*, **272**, 286
- Gügercinoğlu E., 2017, *MNRAS*, **469**, 2313
- Gügercinoğlu E., Alpar M. A., 2014, *ApJ*, **788**, L11
- Gügercinoğlu E., Alpar M. A., 2016, *MNRAS*, **462**, 1453
- Gügercinoğlu E., Alpar M. A., 2020, *MNRAS*, **496**, 2506
- Gügercinoğlu E., Köksal E., Güver T., 2022a, arXiv e-prints, p. arXiv:2207.04111
- Gügercinoğlu E., Ge M. Y., Yuan J. P., Zhou S. Q., 2022b, *MNRAS*, **511**, 425
- Gügercinoğlu E., Alpar M. A., 2017, *MNRAS*, **471**, 4827
- Gügercinoğlu E., Alpar M. A., 2019, *MNRAS*, **488**, 2275
- Ho W. C. G., Espinoza C. M., Antonopoulou D., Andersson N., 2015, *Science Advances*, **1**, e1500578
- Hobbs G. B., Edwards R. T., Manchester R. N., 2006, *MNRAS*, **369**, 655
- Hobbs G., Lyne A. G., Kramer M., 2010, *MNRAS*, **402**, 1027
- Hobbs G., et al., 2011, *Publ. Astron. Soc. Australia*, **28**, 202
- Hotan A. W., van Straten W., Manchester R. N., 2004, *Publ. Astron. Soc. Australia*, **21**, 302
- Jankowski F., et al., 2019, *MNRAS*, **484**, 3691
- Johnston S., Galloway D., 1999, *MNRAS*, **306**, L50
- Jones P. B., 1990, *MNRAS*, **246**, 364
- Karastergiou A., Roberts S. J., Johnston S., Lee H., Weltevrede P., Kramer M., 2011, *MNRAS*, **415**, 251
- Keith M. J., Shannon R. M., Johnston S., 2013, *MNRAS*, **432**, 3080
- Kerr M., Hobbs G., Johnston S., Shannon R. M., 2016, *MNRAS*, **455**, 1845
- Kou F., Yuan J. P., Wang N., Yan W. M., Dang S. J., 2018, *MNRAS*, **478**, L24

- Lander S. K., Andersson N., Antonopoulou D., Watts A. L., 2015, *MNRAS*, **449**, 2047
- Large M. I., Vaughan A. E., Wielebinski R., 1968, *Nature*, **220**, 753
- Link B., Epstein R. I., 1996, *ApJ*, **457**, 844
- Link B., Epstein R. I., 1997, *ApJ*, **478**, L91
- Liu H.-Y., Zhou S.-Q., Zhang Y.-Q., Feng Z.-W., Zhou X., 2021a, *RAA*, **21**, 154
- Liu J., Wang H.-G., Yan Z., Shen Z.-Q., Tong H., Huang Z.-P., Zhao R.-S., 2021b, *ApJ*, **912**, 58
- Liu J., Wang H.-G., Shen Z.-Q., Yan Z., Tong H., Huang Z.-P., Zhao R.-S., 2022, *ApJ*, **931**, 103
- Lower M. E., et al., 2020, *MNRAS*, **494**, 228
- Lower M. E., et al., 2021, *MNRAS*, **508**, 3251
- Lyne A., Hobbs G., Kramer M., Stairs I., Stappers B., 2010, *Science*, **329**, 408
- Maciesiak K., Gil J., 2011, *MNRAS*, **417**, 1444
- Manchester R. N., 2017, *Proc. Int. Astron. Union*, **13**, 197
- Manchester R. N., Hobbs G., 2011, *ApJ*, **736**, L31
- Manchester R. N., Newton L. M., Hamilton P. A., Goss W. M., 1983, *MNRAS*, **202**, 269
- Manchester R. N., Hobbs G. B., Teoh A., Hobbs M., 2005, *AJ*, **129**, 1993
- McCulloch P. M., Hamilton P. A., McConnell D., King E. A., 1990, *Nature*, **346**, 822
- McKenna J., Lyne A. G., 1990, *Nature*, **343**, 349
- Montoli A., Antonelli M., Magistrelli F., Pizzochero P. M., 2020, *A&A*, **642**, A223
- Ng C. W., Takata J., Cheng K. S., 2016, *ApJ*, **825**, 18
- Page D., Geppert U., Weber F., 2006, *Nuclear Phys. A*, **777**, 497
- Palfreyman J., Dickey J. M., Hotan A., Ellingsen S., van Straten W., 2018, *Nature*, **556**, 219
- Philippov A., Tchekhovskoy A., Li J. G., 2014, *MNRAS*, **441**, 1879
- Posselt B., et al., 2021, *MNRAS*, **508**, 4249
- Rankin J. M., 1990, *ApJ*, **352**, 247
- Rencoret J. A., Aguilera-Gómez C., Reisenegger A., 2021, *A&A*, **654**, A47
- Ruderman M., 1976, *ApJ*, **203**, 213
- Ruderman M., Zhu T., Chen K., 1998, *ApJ*, **492**, 267
- Sedrakian A., Cordes J. M., 1999, *MNRAS*, **307**, 365
- Sedrakian A. D., Sedrakian D. M., 1993, *ApJ*, **413**, 658
- Seveso S., Pizzochero P. M., Grill F., Haskell B., 2016, *MNRAS*, **455**, 3952
- Shabanova T. V., 2007, *Ap&SS*, **308**, 591
- Shang X., Li A., 2021, *ApJ*, **923**, 108
- Shaw B., et al., 2018, *MNRAS*, **478**, 3832
- Shaw B., et al., 2022, *MNRAS*, arXiv:2204.10767v2
- Shemar S. L., Lyne A. G., 1996, *MNRAS*, **282**, 677
- Sourie A., Chamel N., 2020, *MNRAS*, **493**, L98
- Takata J., et al., 2020, *ApJ*, **890**, 16
- Warszawski L., Melatos A., Berloff N. G., 2012, *Phys. Rev. B*, **85**, 104503
- Weltevrede P., Johnston S., Espinoza C. M., 2011, *MNRAS*, **411**, 1917
- Yakovlev D. G., Pethick C. J., 2004, *ARA&A*, **42**, 169
- Yi S.-X., Zhang S.-N., 2015, *MNRAS*, **454**, 3674
- Yu Y.-B., Huang Y.-F., 2016, *RAA*, **16**, 75
- Yu M., et al., 2013, *MNRAS*, **429**, 688
- Yuan J. P., Wang N., Manchester R. N., Liu Z. Y., 2010a, *MNRAS*, **404**, 289
- Yuan J. P., Manchester R. N., Wang N., Zhou X., Liu Z. Y., Gao Z. F., 2010b, *ApJ*, **719**, L111
- Yuan J. P., Manchester R. N., Wang N., Wang J. B., Zhou X., Yan W. M., Liu Z. Y., 2017, *MNRAS*, **466**, 1234
- Zhao J., et al., 2017, *ApJ*, **842**, 53
- Zhou S. Q., et al., 2019, *Ap&SS*, **364**, 173
- Zou W. Z., Wang N., Wang H. X., Manchester R. N., Wu X. J., Zhang J., 2004, *MNRAS*, **354**, 811